Structure and Function Characterization of the a1a2 Motifs of *Streptococcus pyogenes* M Protein in Human Plasminogen Binding

Adam J.H. Quek[1], Blake A. Mazzitelli[1], Guojie Wu[1], Eleanor W.W. Leung[1], Tom T. Caradoc-Davies[1,2], Gordon J. Lloyd[1], Devadharshini Jeevarajah[1], Paul J. Conroy[1], Martina Sanderson-Smith[3], Yue Yuan[4], Yetunde A. Ayinuola[4], Francis J. Castellino[4], James C. Whisstock[1,5,†] and Ruby H.P. Law[1,†]

1 - ARC Centre of Excellence in Advanced Molecular Imaging, *Department of Biochemistry and Molecular Biology, Monash Biomedicine Discovery Institute, Monash University, Clayton, Victoria 3800, Australia*
2 - Australian Synchrotron, *800 Blackburn Road, Clayton, Victoria 3168, Australia*
3 - School of Chemistry and Molecular Bioscience, *University of Wollongong, and Illawarra Health and Medical Research Institute, Wollongong, New South Wales 2522, Australia*
4 - W.M. Keck Center for Transgene Research, *University of Notre Dame, Notre Dame, IN 46556, USA*
5 - South East University-Monash Joint Institute, *Institute of Life Sciences, Southeast University, Nanjing 210096, China*

Correspondence to James C. Whisstock and Ruby H.P. Law: *ARC Centre of Excellence in Advanced Molecular Imaging, Department of Biochemistry and Molecular Biology, Monash Biomedicine Discovery Institute, Monash University, Clayton, Victoria 3800, Australia. James.Whisstock@monash.edu, Ruby.Law@monash.edu*
https://doi.org/10.1016/j.jmb.2019.07.003
Edited by Georg Schulz

Abstract

Plasminogen (Plg)-binding M protein (PAM) is a group A streptococcal cell surface receptor that is crucial for bacterial virulence. Previous studies revealed that, by binding to the kringle 2 (KR2) domain of host Plg, the pathogen attains a proteolytic microenvironment on the cell surface that facilitates its dissemination from the primary infection site. Each of the PAM molecules in their dimeric assembly consists of two Plg binding motifs (called the a1 and a2 repeats). To date, the molecular interactions between the a1 repeat and KR2 have been structurally characterized, whereas the role of the a2 repeat is less well defined. Here, we report the 1.7-Å x-ray crystal structure of KR2 in complex with a monomeric PAM peptide that contains both the a1 and a2 motifs. The structure reveals how the PAM peptide forms key interactions simultaneously with two KR2 via the high-affinity lysine isosteres within the a1a2 motifs. Further studies, through combined mutagenesis and functional characterization, show that a2 is a stronger KR2 binder than a1, suggesting that these two motifs may play discrete roles in mediating the final PAM-Plg assembly.

Introduction

Group A streptococcus (GAS) is a human pathogen that causes a range of clinical conditions from superficial skin and pharyngeal infections to much more serious conditions such as rheumatic fever, necrotizing fasciitis, and streptococcal toxic shock [1]. There are over 600 million cases of GAS infection reported each year, which pose significant global economic and healthcare burdens [2]. GAS expresses a number of virulence factors to colonize host tissues [3], disseminate from primary infection sites [4,5], and evade host immune surveillance [3,6]. One of the key virulence determinants is the surface-bound M protein [7,8].

M proteins are typically α-helical coiled-coil proteins consisting of a hypervariable N-terminal region, followed by variable A and B repeat domains, and the conserved C repeats and D domain [9]. There are more than 250 M proteins documented to date via sequence analysis of the hyper-variable N-terminal region [10]. Plasminogen-binding group A streptococcal M-like protein (PAM) belongs to a subgroup of the M protein family with the Plg binding

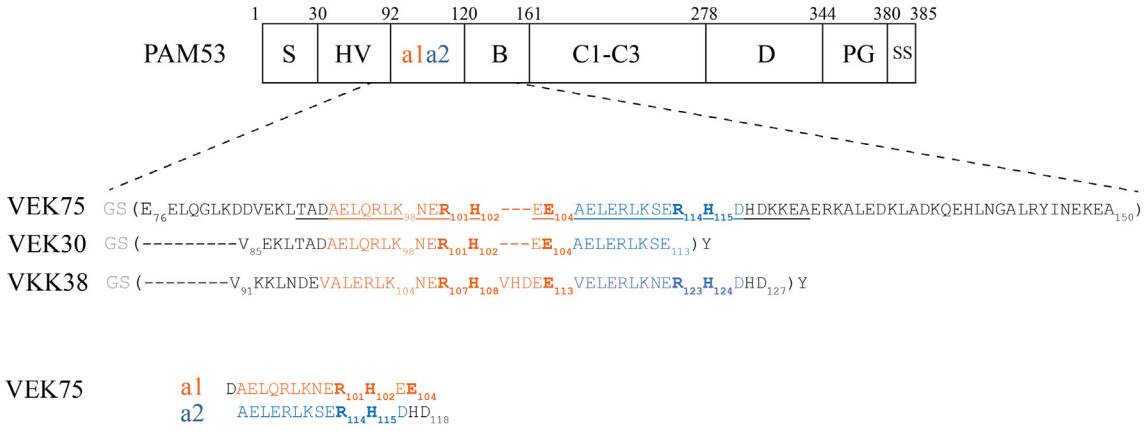

Fig. 1. Schematics of PAM and domains. (a) The domains of PAM from GAS strain AP53 (PAM53) and the sequence alignment of PAM peptides discussed in this article are shown. The N-terminal signal peptide (S) is followed by the hypervariable region (HV), a1a2 repeats, B domain, C1–C3 repeats, D domain, Pro-Gly rich (PG) domain, and LPXTG sortase signal (SS). Shown in the sequence alignment are VEK75 and VEK30 peptides from PAM53 and VKK38 from GAS strain NS455. The a1 and a2 repeats are highlighted in yellow-orange and blue, respectively, with their RH motifs shown in bold. The first and last amino acids of each peptide and the RH motifs are numbered. Underlined are the residues modeled in the VEK75–KR2 crystal structure described in the current study. Residues colored in gray are those of the thrombin cleavage site. (b) Sequence alignment of the a1 and a2 repeat in VEK75.

a1a2 repeat located at the variable A domain [11]. PAM on the bacterial surface recruits plasminogen (Plg) and facilitates the formation of plasmin (Plm) by streptokinase, a plasminogen activator also secreted by GAS, thus enabling the pathogen to disseminate from the primary infection site and recolonize within the host [12].

Plg, the inactive precursor of the protease Plm [13,14], is a 92-kDa multi-domain glycoprotein. It consists of seven domains, an N-terminal PAN-apple (PAp) domain followed by five homologous kringle (KR1–5) domains, and a C-terminal serine protease (SP) domain. All KR domains, except for KR3, have a functional lysine-binding site (LBS: Asp-X-Asp for KR1, 4–5, and Asp-Arg-Glu for KR2) that binds to C-terminal lysine or internal lysine or arginine residues present on target substrates or receptors [14]. Previous crystallographic and NMR studies on VEK30, an internal peptide with the a1 repeat from PAM53 (GAS strain AP53, Fig. 1), revealed that it binds to the lysine binding site (LBS) of Plg KR2 via an internal lysine isostere site on the peptide [15–17]. Specifically, VEK30 binds to KR2 via the key residues Arg_{101}^{VEK30} and His_{102}^{VEK30} (hence, it is also called the RH motif, Fig. 1) [15,16,18]. Intriguingly, PAM53, as well as many PAM variants [19], has a second RH motif (RH2) located at the a2 repeat. A recent study on a peptide called VKK38 (isolated from GAS strain NS455, Fig. 1), which contains both the a1 and a2 repeats with a 3-residue insertion (Val_{109}–His_{110}–Asp_{111}) between the repeats, suggested that the RH2 motif is also a KR2 binder [20] and that both RH motifs are located at the disordered regions of the apo-peptide. Using combined analytical ultracentrifugation, isothermal titration calorimetry, and NMR, this study further suggested that VKK38 binds to two KR2 domains in solution. Exactly how the RH motifs interact with two KR2 domains simultaneously and their molecular interaction remain to be fully elucidated experimentally.

In the present study, we report a 1.7-Å co-crystal structure of VEK75 (an a1a2 containing peptide from PAM53 residues 76–150 [21]; Fig. 1) simultaneously bound to two molecules of KR2, which contains its native LBS motif, confirming the aforementioned VKK38 data. We further characterize the functional and binding affinity of RH1 and RH2 for Plg using enzyme kinetics and surface plasmon resonance (SPR) studies on the RH deletion mutants. Our results reveal unexpectedly that RH2 has a higher affinity for Plg than RH1, suggesting that a1 and a2 might play a different role in the final PAM-Plg binary complex.

Table 1. Comparison of the molar masses of VEK75, KR2 and VEK75–KR2 complex derived from MALS and the molar masses calculated based on amino acid sequences (Protparam, Expasy server)

	Experimental mass (kDa)	Calculated mass (kDa)
VEK75	8.94 ± 0.89	9.02
KR2	13.09 ± 0.79	13.19
VEK75–KR2	31.74 ± 0.98	35.38[a]

[a] Predicted molar mass for VEK75:KR2 molar ratio of 1:2.

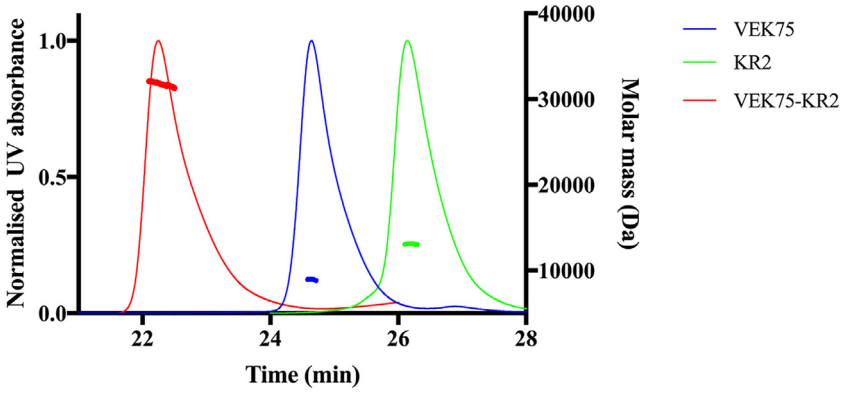

Fig. 2. SEC-MALS analysis. SEC-MALS analysis of VEK75 (blue), KR2 (green), and VEK75–KR2 complex (red). Note that despite its smaller mass, VEK75 elutes earlier than KR2, presumably due to its relaxed molecular shape. Molar masses obtained are tabulated in Table 1.

Results

Stoichiometry of VEK75–KR2 complex

Size exclusion chromatography (AdvanceBio SEC 300 Å column; Agilent) combined with multi-angle light scattering (SEC-MALS) was used to determine the molecular masses of VEK75, KR2, and VEK75–KR2 complex in solution. The SEC-MALS studies reveal that VEK75 is a monomer in solution (8.94 ± 0.89 kDa; Table 1 and Fig. 2) instead of a weakly associated dimer as reported previously [21]; KR2 is also a monomer in solution (13.09 ± 0.79 kDa) as expected. The molar mass of VEK75–KR2 complex is 31.74 ± 0.98 kDa. The closest assembly would consist of two copies of KR2 bound to one VEK75 (expected molar mass of 35.38 kDa).

Crystal structure of VEK75–KR2 complex

Previous studies on the binary complexes of VEK30–KR2 and VEK30–angiostatin (PDB ID: 1I5K, 2DOH, and 2DOI) [15,16] revealed that KR2 anchors to the a1 region of PAM via the RH1 (Arg_{101} and His_{102}) together with the residues Lys_{98} and Glu_{104} on either side of the RH motif.

The present crystal structure (Fig. 3a and Table S1) of the VEK75–KR2 complex is a ternary structure consisting of one VEK peptide with two KR2 molecules, which is accordingly in agreement with the above SEC-MALS data and also the VKK38 studies [20]. The first KR2 (termed KR2a) forms interactions with the RH1 motif (residues 92–104; Figs. 1b, 3b, and S3a) [15,16], while the second KR2 (termed KR2b) binds to the RH2 motif of a2 (residues 105–116; Figs. 1b, 3c, and S3b) [20]. Both KR2 molecules bind to the lysine isosteres on opposite sides of the α-helical peptide and are separated by 3.6 helical turns.

In the crystal structure, 34 residues of VEK75 (residue 89–122, underlined in Fig. 1a) adopt an end-to-end α-helical structure and are well resolved in the electron density map. In the a1 repeat, Arg_{96}^{VEK75} forms side-chain salt bridges with Glu_{93}^{VEK75} (Fig. S1a), whereas in the a2 repeat, residue Arg_{109}^{VEK75} forms side-chain salt bridges with Glu_{106}^{VEK75} as well as Glu_{113}^{VEK75} (Fig. S1b). No other intramolecular side-chain interaction is observed within the structure of VEK75.

The remaining 43 residues of the VEK75 peptide (15 of the N-terminal and 28 of the C-terminal residues) outside the KR2 binding sites could not be modeled into the electron density. Mass spectrometry studies on the VEK75–KR2 co-crystals (~6 weeks post-purification) (Fig. S2) revealed that 11 residues were missing from the VEK75 peptide (3 and 8 residues from N- and C-terminus, respectively), with all the other residues remaining intact. Taken together, these data suggest that residues flanking the KR2 binding sites are structurally disordered. Similar observations have been reported on the solution structure of VKK38 determined by NMR [20].

Structural alignment of the two KR2s suggests that they are essentially identical (r.m.s.d. = 0.199 over 492 atoms) (Fig. S1c). Both molecules bind to a sulfate ion, present in the crystallization solution (Fig. S1d). The biggest main chain variation is at residues 202–209 of KR2b, where Pro_{206}^{KR2} moved by 1 Å (Fig. S1c). This structural difference is a result of an extra H-bond formed between residues Lys_{204}^{KR2b} and Glu_{106}^{VEK75} (Fig. 3c) that is not found in the equivalent position of KR2a (equivalent residues are Lys_{204}^{KR2a} and Glu_{93}^{VEK75}; Fig. 1b). The C-terminal c-myc and hexahistidine tags of KR2 could not be modeled into the density. Analysis of the crystal by SDS-PAGE (data not shown) and mass spectrometry (Fig. S2) indicated that the tags were absent from the protein sequence, presumably as a result of proteolytic degradation.

Intermolecular interactions between a1 and KR2a *versus* a2 and KR2b

The molecular interactions between a1/a2 and KR2 are different (Table S2). Specifically, residues

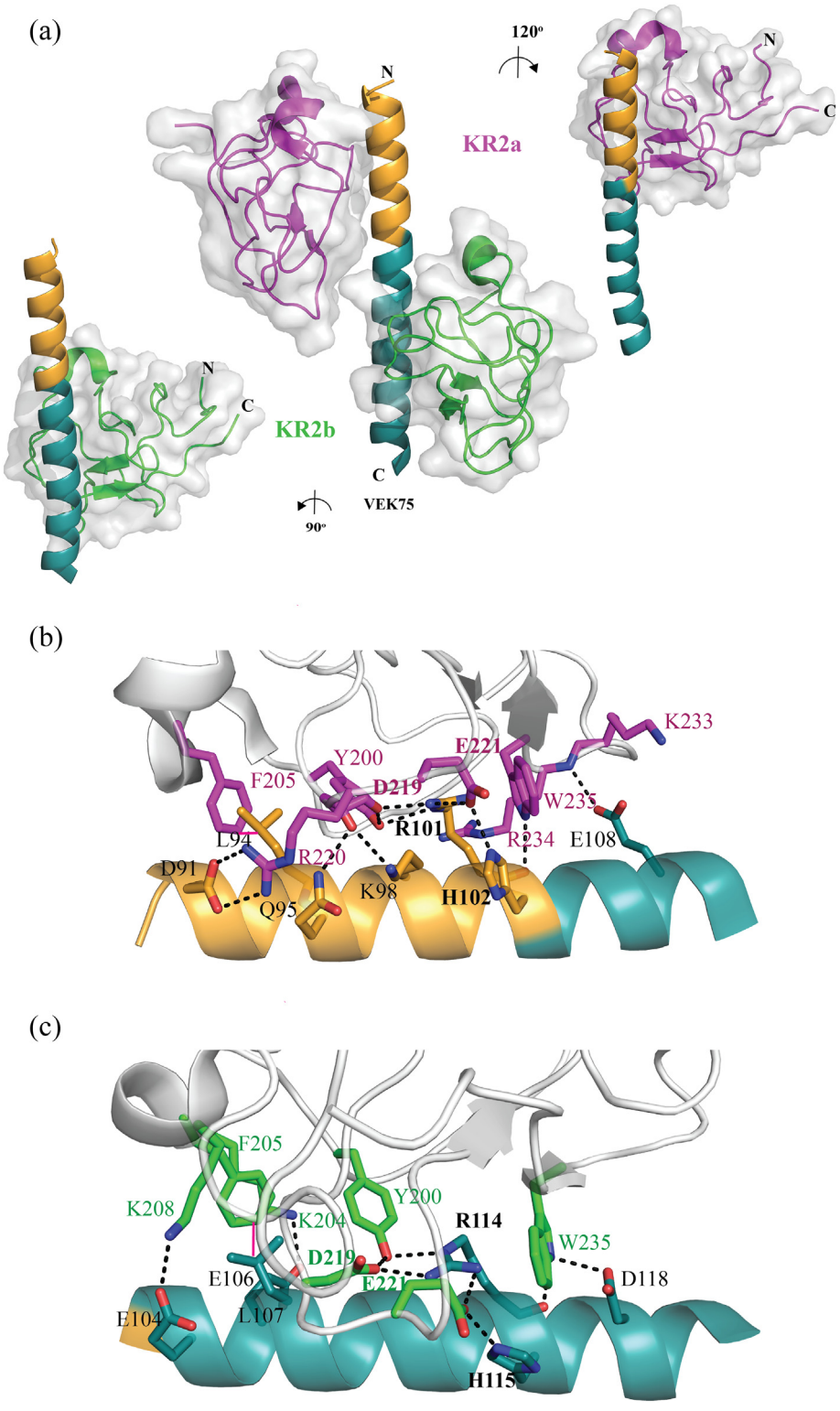

Fig. 3 (*legend on next page*)

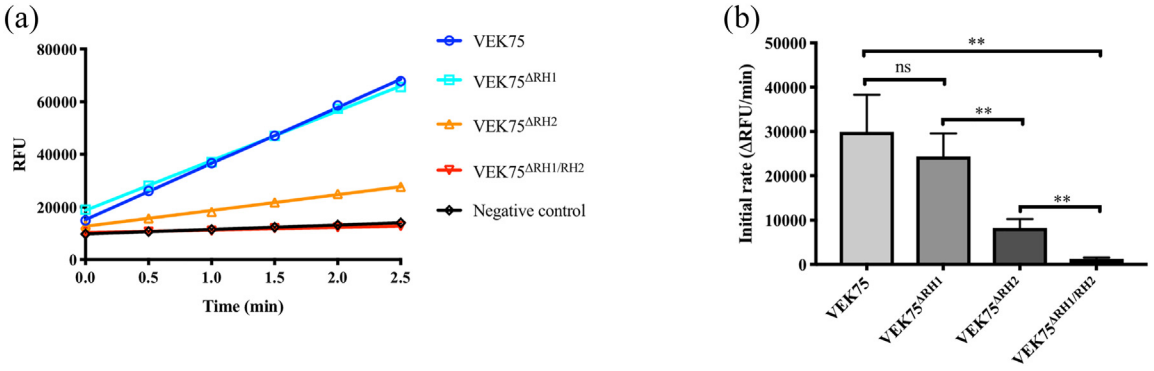

Fig. 4. Plasminogen activation assay. (a) A representative plasminogen activation assay in the presence of VEK75 and RH mutants. VEK75 was not added to the negative control. RFU: relative fluorescence unit. (b) Initial rate comparison correlating to plasmin generation in the presence of VEK75 and RH mutants. Data represent mean values from three independent experiments, and error bars represent S.E.M. Statistical significance was determined by unpaired Student's *t* test. $^{**}p < 0.01$; ns: not statistically significant.

between Asp_{91}^{VEK75} and Glu_{108}^{VEK75} bind to the LBS of KR2a forming an extensive network of direct interactions (Fig. 3b and S3a), as previously reported [16]. Outside the LBS, other interactions observed in the structure are found between VEK75 and KR2a as shown in Fig. 3b. Here, residue Glu_{108}^{VEK75}, which is also a part of the a2 repeat, forms H-bonds with KR2a and is unique to the VEK75–KR2a interaction. Further to these direct interactions, there are three additional interactions mediated by water molecules (Fig. S3c). At the a1–KR2a interface, the total buried surface is 613.1 $Å^2$ with a ΔG of −0.5 kcal/mol.

VEK75 binds to KR2b via residues Glu_{104}^{VEK75} and Asp_{118}^{VEK75} (Fig. 1b); in particular, the LBS of KR2b also forms an extensive network of direct interactions with residues of the RH2 motif (Figs. 3c and S3b) similar to that of KR2a but with three additional interactions unique to a2 and KR2b as shown in Fig. 3c. The interaction formed between Glu_{104}^{VEK75}/Lys_{208}^{KR2b} is about three helical turns upstream of the His_{115}^{VEK75} of the RH2 motif (Fig. 3c), and its involvement in VEK binding has not been reported previously. An additional interaction between Glu_{106}^{VEK75}/Lys_{204}^{KR2b} leads to the structural variation between KR2a and KR2b observed at residues 202–209 described above. Compared to RH1 and KR2a, three more (a total of six) water-mediated interactions are seen here at the RH2–KR2b interface (Fig. S3c and d). Although the total buried surface area of the a2–KR2b interaction is similar to that of a1–KR2a, at 564.6 $Å^2$, the ΔG (−2.2 kcal/mol) is four times higher than that of the a1–KR2a. Accordingly, our structural data suggest that a2 is the high-affinity site.

Taken together, the VEK75 peptide was crystallized in its monomeric form with one molecule of KR2 bound to a1 and the other to the a2 repeat. The two KR2 molecules bound to the helical VEK peptide are 220° or 3.6 helical turns apart, which is comparable to the NMR model of VKK38 [20]. Further analysis on the KR2 binding interface reveals a very distinct charge complementarity in the a1/a2 repeat and KR2 interface (Fig. S4). To date, the functional significance of having both a1 and a2 domains is not well understood. To investigate this further, biochemical and biophysical studies were performed to gain insights into the properties of the a1 and a2 repeats.

Role of RH2 in the activation potential of Plg

The binding of Plg to VEK peptides promotes conformational change, and as a result, the Plg activation loop becomes accessible to Plg activators [21]. Here, enzyme assays were performed to compare the Plg–VEK interactions using mutants generated in this study, namely, $VEK75^{\Delta RH1}$ ($R_{101}A$ and $H_{102}A$), $VEK75^{\Delta RH2}$ ($R_{114}A$ and $H_{115}A$), and $VEK75^{\Delta RH1/RH2}$ ($R_{101}A$, $H_{102}A$, $R_{114}A$, and $H_{115}A$), and the results are compared with that of the wild-type VEK75.

Consistent with current understandings [11], mutating both the RH1 and RH2 motifs in $VEK75^{\Delta RH1/RH2}$

Fig. 3. Cartoon representation of VEK75–KR2 crystal structure. (a) The structure of the VEK75–KR2 complex. VEK75 is colored in yellow-orange and teal to represent the a1 and a2 repeat, respectively. The N and C-termini of the molecules are labeled; KR2a and KR2b are also shown in transparent surface (gray). Interactions between KR2a (magenta) and KR2b (green) with (b) a1 and (c) a2 repeat, respectively, are shown. Asp and Glu residues of the KR2 LBS (Asp_{219}–Arg_{220}–Glu_{221}) and the RH motifs are highlighted in bold font. Salt bridge and hydrogen bond are shown as dashed lines, and Van Der Waals interaction is shown as red line.

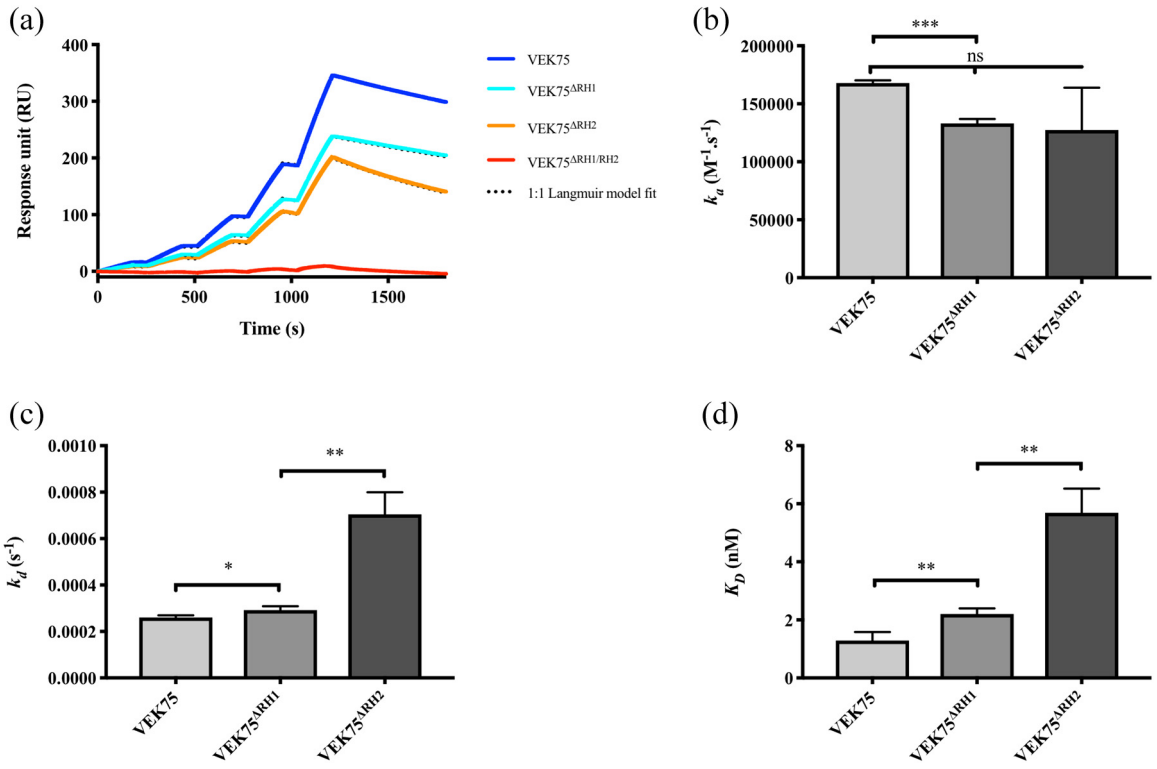

Fig. 5. SPR experiments. SPR binding assays of Plg to VEK75 and RH motif mutants. (a) The binding of Plg (0.625 to 10 nM) to immobilized VEK75 and RH mutants was monitored via single-cycle kinetics experiment. The sensorgrams were fitted using a 1:1 Langmuir binding model. Kinetic constants k_a (b) and k_d (c) derived are compared between VEK75 and RH mutants. (d) Overall affinity constant (K_D) of VEK75 and RH mutants for Plg. Data represent mean and S.E.M. values from three independent experiments. Statistical significance was determined by unpaired Student's *t* test. $^*p < 0.05$; $^{**}p < 0.01$; $^{***}p < 0.001$; ns: not statistically significant.

completely abolishes VEK75-dependent Plg activation (Fig. 4a). Interestingly, while the activity of VEK75$^{\Delta RH1}$ is comparable to that of VEK75, VEK75$^{\Delta RH2}$ shows ~3-fold lower activity [24.3 ± 3.1 RFU/min ($\times 10^3$) and 8.3 ± 1.1 RFU/min ($\times 10^3$), respectively; Fig. 4b]. Based on these observations, we confirm that the RH2 is the dominant and higher affinity site of the two RHs. To further verify this hypothesis, we assessed the affinity of Plg for VEK75 and the RH mutants by SPR.

RH2 is important for the stability of the VEK75–Plg complex

Single-cycle SPR experiments were carried out with VEK75 and mutants immobilized on a NiHC 1000 M chip (Xantec, Germany) followed by five injections of Plg (0.625 nM to 10 nM; Fig. 5a). Consistent with the Plg activation studies discussed above, no Plg binding to VEK75$^{\Delta RH1/RH2}$ is detectable. Although the k_a of VEK75 is marginally higher than that of VEK75$^{\Delta RH1}$ (Fig. 5b and Table 2), the overall affinity increases in the order of VEK75$^{\Delta RH2}$ < VEK75$^{\Delta RH1}$ < VEK75 (K_D of 5.69 ± 0.48, 2.20 ± 0.11 and 1.29 ± 0.12 nM, respectively) (Fig. 5d and Table 2). Interestingly, the dissociation constant (k_d) for VEK75$^{\Delta RH2}$ (7.05 ± 0.55 s^{-1} ($\times 10^{-4}$)) is higher than that of VEK75 and VEK75$^{\Delta RH1}$ (2.61 ± 0.05 and 2.92 ± 0.10 s^{-1} ($\times 10^{-4}$), respectively; Fig. 5c]. This observation confirms further that RH2 plays a dominant role in stabilizing the Plg–VEK75 complex.

Table 2. Affinity constants (K_D) of the binding of VEK75 and RH motif mutants to Plg

	k_a (M^{-1} s^{-1}) × 10^5	k_d (s^{-1}) × 10^{-4}	K_D (nM)
VEK75	1.68 ± 0.01	2.61 ± 0.05	1.29 ± 0.12
VEK75$^{\Delta RH1}$	1.33 ± 0.02	2.92 ± 0.10	2.20 ± 0.11
VEK75$^{\Delta RH2}$	1.27 ± 0.21	7.05 ± 0.55	5.69 ± 0.48
VEK75$^{\Delta RH1/\Delta RH2}$	Not determined		

k_a, k_d, and K_D values represent mean ± S.E.M. of data obtained from three independent experiments.

Discussion

PAM is a key virulence factor of skin-tropic GAS strains and also the highest-affinity Plg receptor described [20,22]. Despite its pathological significance, the structural details of the full-length PAM and how it binds to Plg are not known. Prior to this study, the binding of a1 to KR2 has been well documented [15,16,23,24]; however, the molecular interactions between a2 and KR2 have not been defined in detail experimentally.

The x-ray crystal structure provides the atomic details of the interaction between the VEK75 peptide with two KR2 molecules. Furthermore, structural analysis revealed that a2 has a 5-fold higher affinity for KR2 than a1 (ΔG of −0.4 kcal/mol and −2.6 kcal/mol for a1 and a2, respectively). This was further supported by biophysical and biochemical experiments (Figs. 4 and 5); specifically, in both assays, the affinity of VEK75$^{\Delta RH1}$ for Plg is ~3 times higher than that of VEK75$^{\Delta RH2}$.

Unlike the A and B fragment from the serotype M1 protein, which adopts an parallel dimeric coiled-coild structure (PDB ID 2OTO) [25], recent NMR studies [25] revealed that in solution, the structure of apo-VEK75 consists of short segments of helical structures connected by random coils instead of the long helix observed in the crystal structure. High resolution NMR studies on VKK38 further revealed that the RH motifs are located at random coiled regions, which are separated by a short helix, indicating that KR2 binding promotes a significant conformational change [20].

Structural comparison between the crystal and solution structures suggests that residues 89–122 in VEK75 transform to an extended helical structure upon its binding to the KR2s. Specifically, in the apo-VEK75, RH motifs at the flexible loop region are expected to facilitate the initial docking of KR2 via the LBS to the peptide. Subsequent interaction of the vicinal residues outside the RH and LBS leads to the conformational change of VEK75 from a flexible to a helical structure. In support of this notion, there are eight direct interactions flanking the RH motifs observed between VEK75 and KR2a, and four between VEK75 and KR2b. These interactions, together with water-mediated interactions at each binding interface, are expected to facilitate the conformational change of VEK75 upon binding to KR2 and stabilize the complex formed (Fig. S3c and d). Although the VEK75 molecule was found to be 11 amino acids shorter than the starting material in the crystal (based on mass spectrometry studies), a total of 43 residues outside the two KR2 binding regions cannot be modeled into the electron density. This suggests that VEK75 sequences outside the KR2 binding sites remain highly flexible. Further structural studies will unveil whether the proposed two-step binding mode of KR2 to VEK75 is legitimate and also takes place in the binding of Plg to other receptors without a C-terminal lysine residue.

Further to the induction of conformational change in VEK75 by KR2 binding and the new structural information on the interactions between KR2b and RH2, another insightful observation gained in the current study is from the enzyme kinetic studies and SPR experiments performed using the ΔRH mutants. The results show that the RH2 motif plays a more important role in both VEK75 mediated Plg activation and the stability of the VEK75–Plg complex.

Based on the structural data, interactions between a1 with KR2a and a2 with KR2b are structurally different and highly specific, such that a2 and KR2b form two unique intermolecular interactions, one between $Glu_{106}^{VEK75}/Lys_{204}^{KR2b}$ and the other between $Glu_{104}^{VEK75}/Lys_{208}^{KR2b}$. Sequence alignment of human Plg kringle domains showed that Lys_{204}^{KR2} is only found in KR2, whereas Lys_{208}^{KR2} is also found in KR3 (Fig. S5). Further comparison of the crystal contacts between the two sites reveals that Arg_{220}^{KR2a} (which is only found in KR2, Fig. S5) is heavily involved in the a1 interactions via residues Asp_{91}^{VEK75}, Gln_{95}^{VEK75}, and Lys_{98}^{VEK75} but does not play any role in the intermolecular interaction between KR2b and a2 repeat. Structural alignment of the current crystal structure with full-length Plg [14] excludes the possibility that a VEK peptide can bind simultaneously to two full-length Plg because of steric clashes. The observation that RH1 and RH2 each binds to a separate KR2 suggests that this may represent two different Plg binding modes, or alternatively, one of two RHs actually binds to a non-KR2 kringle domain in the final complex [26]. Further structural studies using full-length PAM and Plg would be essential to address these questions.

Materials and Methods

Mutagenesis and protein purification

Recombinant VEK75 fused to the B1 domain of streptococcal G protein (GB1) is expressed using the pET-15b plasmid (Fig. S6a). RH1 and RH2 mutations were introduced using primers listed in Table S3 and a standard Quikchange site-directed mutagenesis protocol. Using RH1 mutant (VEK75$^{\Delta RH1}$) as the DNA template, RH2 mutation was introduced to obtain VEK75$^{\Delta RH1/RH2}$. Mutations were verified by Sanger sequencing (Micromon DNA Sequencing Facility, Monash University). VEK75 and mutants

were expressed in *Escherichia coli* and purified as previously described [21].

Recombinant human KR2 with a C169A mutation (Fig. S6b) in pSecTag2a was expressed in Expi293 cells as a C-terminal c-myc-hexahistidine fusion protein (Thermo Fisher Scientific) according to the manufacturer's recommendations. KR2 was purified from the culture supernatant using Ni^{2+} Sepharose (GE Healthcare) followed by size-exclusion chromatography using a Superdex 75 16/60 (GE Healthcare) in a buffer containing 25 mM Hepes–NaOH and 150 mM NaCl (pH 7.4). Human Plg was purified from human plasma as described previously [28].

When required, protein samples were concentrated at 4 °C by ultrafiltration and concentrations were determined by UV absorbance using the extinction coefficients of 1490, 21,345, and 152,200 M^{-1} cm^{-1} for VEK75, KR2, and Plg, respectively.

SEC-MALS

Samples were purified through an AdvanceBio SEC 300 Å column (Agilent) in a buffer containing 25 mM Hepes–NaOH and 150 mM NaCl (pH 7.4) and analyzed immediately using the DAWN HELEOS light-scattering detector, an Optilab T-rEX differential refractive-index detector and a quasi-elastic light-scattering detector (Wyatt Technology Corporation). The light scattering intensity and refractive index profiles were analyzed using ASTRA 6.0 (Wyatt Technology Corporation). Data were exported and plotted using GraphPad Prism 8.0 (GraphPad).

Crystallization of the VEK75–KR2 complex

An excess amount of KR2 was mixed with VEK75 for at least 30 min at room temperature prior to purification using a size exclusion column (Superdex 75 16/60; GE Healthcare). The peak obtained, consisting of the stable complex of VEK75–KR2 obtained, was pooled and concentrated to 10 mg/ml in a centrifugal filter. Crystals of VEK75–KR2 were obtained by sitting drop vapor diffusion at 20 °C in the presence of 0.1 M Hepes (pH 7.0) and 2 M ammonium sulfate after 6 weeks of incubation.

Collection of diffraction data

Crystals of VEK75–KR2 were flash cooled with liquid N_2 in the presence of 20% glycerol as a cryo-protectant. Diffraction data were collected at MX2 beamline of the Australian Synchrotron [27].

Structure determination and refinement

The structure was determined by molecular replacement using PHASER [28] and KR2 from the crystal structure of full-length human plasminogen (PDB ID: 4DUR) [14] and VEK30 from the crystal structure of angiostatin–VEK30 (PDB ID: 2DOI) [16] as search models. Model building was carried out in COOT [29], and refinement was done first in BUSTER [30] and completed in PHENIX [31]. Data collection and refinement statistics are summarized in Table S1.

Plg activation assay

Human Plg (0.25 μM) was activated by 0.01 μM tissue-type Plg activator (tPA) in the presence of 50 μM VEK75 and RH mutants. tPA was chosen as it is the most sensitive to Plg's conformational state, which is perturbed upon VEK75 binding. No VEK75 was added to the negative control reaction. Plasmin generation at 37 °C was monitored using fluorogenic plasmin substrate H-Ala-Phe-Lys-AMC (Bachem) in a Fluostar Omega plate reader (BMG labtech) via excitation and emission wavelengths of 355 and 460 nm, respectively. The initial rate of reaction, which is proportional to the amount of plasmin generated, was obtained by performing linear regression of the first 2.5 min of the progress curve. Three independent experiments were carried out, and Student's *t* test was used to determine statistical significance of the differences in GraphPad Prism 8.0 (GraphPad Software).

SPR

Hexahistidine-tagged VEK75 was immobilized to an NiHC 1000 M chip (Xantec) and the binding of Plg ranging from 0.625 to 10 nM at 25 °C was analyzed using Biacore T200 (GE Healthcare). In a buffer containing 10 mM Hepes (pH 7.4), 150 mM NaCl, 50 μM EDTA, and 0.05% (v/v) Tween 20, Plg in increasing concentration was injected at 30 μl/min in five successive 180-s cycles followed by a 600-s dissociation cycle. The chip surface was regenerated between cycles by injecting 0.5 M EDTA followed by 2.5 mM $NiCl_2$. Sensorgrams were fitted with 1:1 binding model using Biacore T200 Evaluation software (GE Healthcare). SPR experiments were repeated twice or more, and statistical significance of kinetics and affinity differences were analyzed using the Student's *t* test available in GraphPad Prism 8.0 (GraphPad Software).

Accession numbers

Coordinates and structure factors have been deposited in the Protein Data Bank with accession number 6OG4.

Acknowledgments

The authors thank the Australian Synchrotron for MX2 beamtime and technical assistance, and the Monash Molecular Crystallization Facility for setting up crystallization experiments. This research was undertaken in part using the MX2 beamline at the Australian Synchrotron, part of ANSTO, and made use of the ACRF detector. This work was supported in part by the Australian National Health Medical Research Council. G.W. and B.A.M. are supported by Monash University PhD scholarships, and J.C.W. is an Australian Laureate Research Fellow.

Author Contributions: A.Q. designed and conducted the study and co-wrote the manuscript; B.A.M., G.W., E.W.W.L., G.J.L., D.J., Y.Y., and Y.A. provided input on design of experiments; T.C.D., P.J. C., and M.S.S. provided input on data interpretation and design; F.J.C., J.C.W., and R.H.P.L. designed the study, provided input on data interpretation, and co-wrote the manuscript.

Appendix A. Supplementary data

Supplementary data to this article can be found online at https://doi.org/10.1016/j.jmb.2019.07.003.

Received 2 April 2019;
Received in revised form 28 June 2019;
Accepted 1 July 2019
Available online 8 July 2019

Keywords:
PAM;
plasminogen kringle 2;
RH motif;
lysine-binding site;
a1a2 repeat

†Contributed equally.

References

[1] A.P. Ralph, J.R. Carapetis, Group a streptococcal diseases and their global burden, Curr. Top. Microbiol. Immunol. 368 (2013) 1–27.

[2] Sims Sanyahumbi, A., Colquhoun, S., Wyber, R., and Carapetis, J. R. (2016) Global disease burden of group a streptococcus. In *Streptococcus pyogenes: Basic Biology to Clinical Manifestations* (Ferretti, J. J., Stevens, D. L., and Fischetti, V. A. eds.). Pp 661-704.

[3] N.N. Lynskey, M. Reglinski, D. Calay, M.K. Siggins, J.C. Mason, M. Botto, S. Sriskandan, Multi-functional mechanisms of immune evasion by the streptococcal complement inhibitor C5a peptidase, PLoS Pathog. 13 (2017), e1006493.

[4] Andreoni, F., Ogawa, T., Ogawa, M., Madon, J., Uchiyama, S., Schuepbach, R. A., and Zinkernagel, A. S. (2014) The IL-8 protease SpyCEP is detrimental for group a streptococcus host-cells interaction and biofilm formation. *Frontiers in Microbiology* 5; 339, 1-9.

[5] W.S. Tillett, The fibrinolytic activity of hemolytic streptococci, Bacteriol. Rev. 2 (1938) 161–216.

[6] K. Dinkla, I. Sastalla, A.W. Godehardt, N. Janze, G.S. Chhatwal, M. Rohde, E. Medina, Upregulation of capsule enables *Streptococcus pyogenes* to evade immune recognition by antigen-specific antibodies directed to the G-related alpha2-macroglobulin-binding protein GRAB located on the bacterial surface, Microbes Infect. 9 (2007) 922–931.

[7] V.A. Fischetti, Streptococcal M protein: molecular design and biological behavior, Clin. Microbiol. Rev. 2 (1989) 285–314.

[8] Fischetti, V. A. (2016) M protein and other surface proteins on streptococci. In *Streptococcus pyogenes: Basic Biology to Clinical Manifestations* (Ferretti, J. J., Stevens, D. L., and Fischetti, V. A. eds.). Pp 27-53.

[9] P. Ghosh, Variation, indispensability, and masking in the M protein, Trends Microbiol. 26 (2018) 132–144.

[10] D.J. McMillan, P.A. Dreze, T. Vu, D.E. Bessen, J. Guglielmini, A.C. Steer, J.R. Carapetis, L. Van Melderen, K.S. Sriprakash, P.R. Smeesters, Updated model of group A streptococcus M proteins based on a comprehensive worldwide study, Clinical microbiology and infection: the official publication of the European Society of Clinical Microbiology and Infectious Diseases 19 (2013) E222–E229.

[11] Sanderson-Smith, M. L., Walker, M. J., and Ranson, M. (2006) The maintenance of high affinity plasminogen binding by group A streptococcal plasminogen-binding M-like protein is mediated by arginine and histidine residues within the a1 and a2 repeat domains. *J Biol Chem.* 281, 25965–25971. Epub 22006 Jul 25965.

[12] U. Ringdahl, M. Svensson, A.C. Wistedt, T. Renne, R. Kellner, W. Muller-Esterl, U. Sjobring, Molecular co-operation between protein PAM and streptokinase for plasmin acquisition by *Streptococcus pyogenes*, J. Biol. Chem. 273 (1998) 6424–6430.

[13] F.J. Castellino, J.R. Powell, Human plasminogen, Methods Enzymol. 80 (1981) 365–378.

[14] Law, R. H., Caradoc-Davies, T., Cowieson, N., Horvath, A. J., Quek, A. J., Encarnacao, J. A., Steer, D., Cowan, A., Zhang, Q., Lu, B. G., Pike, R. N., Smith, A. I., Coughlin, P. B., and Whisstock, J. C. (2012) The x-ray crystal structure of full-length human plasminogen. *Cell Rep.* 1, 185–190. doi: 110.1016/j.celrep.2012.1002.1012. Epub 2012 Mar 1018.

[15] J.L. Rios-Steiner, M. Schenone, I. Mochalkin, A. Tulinsky, F.J. Castellino, Structure and binding determinants of the recombinant kringle-2 domain of human plasminogen to an internal peptide from a group A streptococcal surface protein, J. Mol. Biol. 308 (2001) 705–719.

[16] S.E. Cnudde, M. Prorok, F.J. Castellino, J.H. Geiger, X-ray crystallographic structure of the angiogenesis inhibitor, angiostatin, bound to a peptide from the group A streptococcal surface protein PAM, Biochemistry 45 (2006) 11052–11060.

[17] Q. Fu, M. Figuera-Losada, V.A. Ploplis, S. Cnudde, J.H. Geiger, M. Prorok, F.J. Castellino, The lack of binding of VEK-30, an internal peptide from the group A streptococcal M-like protein, PAM, to murine plasminogen is due to two amino acid replacements in the plasminogen kringle-2 domain, J. Biol. Chem. 283 (2008) 1580–1587.

[18] A.C. Wistedt, H. Kotarsky, D. Marti, U. Ringdahl, F.J. Castellino, J. Schaller, U. Sjöbring, Kringle 2 mediates high affinity binding of

plasminogen to an internal sequence in streptococcal surface protein PAM, J. Biol. Chem. 273 (1998) 24420–24424.
[19] M. Sanderson-Smith, M. Batzloff, K.S. Sriprakash, M. Dowton, M. Ranson, M.J. Walker, Divergence in the plasminogen-binding group A streptococcal M protein family: functional conservation of binding site and potential role for immune selection of variants, J. Biol. Chem. 281 (2006) 3217–3226.
[20] Y. Yuan, J. Zajicek, C. Qiu, V. Chandrahas, S.W. Lee, V.A. Ploplis, F.J. Castellino, Conformationally organized lysine isosteres in *Streptococcus pyogenes* M protein mediate direct high-affinity binding to human plasminogen, J. Biol. Chem. 292 (2017) 15016–15027.
[21] Bhattacharya, S., Liang, Z., Quek, A. J., Ploplis, V. A., Law, R., and Castellino, F. J. (2014) Dimerization is not a determining factor for functional high affinity human plasminogen binding by the group A streptococcal virulence factor PAM and is mediated by specific residues within the PAM a1a2 domain. J Biol Chem. 289, 21684-21693. Doi: 21610.21074/jbc. M21114.570218. Epub 572014 Jun 570224.
[22] E.F. Plow, L. Doeuvre, R. Das, So many plasminogen receptors: why? J. Biomed. Biotechnol. 2012 (2012) 141806.
[23] M. Figuera-Losada, M. Ranson, M.L. Sanderson-Smith, M.J. Walker, F.J. Castellino, M. Prorok, Effects on human plasminogen conformation and activation rate caused by interaction with VEK-30, a peptide derived from the group A streptococcal M-like protein (PAM), Biochimica et Biophysica Acta - Proteins and Proteomics 1804 (2010) 1342–1349.
[24] Wang, M., Prorok, M., and Castellino, F. J. (2010) NMR backbone dynamics of VEK-30 bound to the human plasminogen kringle 2 domain. *Biophys J.* 99, 302-312. Doi: 310.1016/j.bpj.2010.1004.1019.
[25] C. Qiu, Y. Yuan, J. Zajicek, Z. Liang, R.D. Balsara, T. Brito-Robionson, S.W. Lee, V.A. Ploplis, F.J. Castellino, Contributions of different modules of the plasminogen-binding *Streptococcus pyogenes* M-protein that mediate its functional dimerization, J. Struct. Biol. 204 (2018) 151–164.
[26] M.L. Hayes, F.J. Castellino, Carbohydrate of the human plasminogen variants. I. Carbohydrate composition, glycopeptide isolation, and characterization, J. Biol. Chem. 254 (1979) 8768–8771.
[27] D. Aragao, J. Aishima, H. Cherukuvada, R. Clarken, M. Clift, N. P. Cowieson, D.J. Ericsson, C.L. Gee, S. Macedo, N. Mudie, S. Panjikar, J.R. Price, A. Riboldi-Tunnicliffe, R. Rostan, R. Williamson, T.T. Caradoc-Davies, MX2: a high-flux undulator microfocus beamline serving both the chemical and macromolecular crystallography communities at the Australian Synchrotron, J. Synchrotron Radiat. 25 (2018) 885–891.
[28] A.J. McCoy, R.W. Grosse-Kunstleve, P.D. Adams, M.D. Winn, L.C. Storoni, R.J. Read, Phaser crystallographic software, J. Appl. Crystallogr. 40 (2007) 658–674.
[29] P. Emsley, B. Lohkamp, W.G. Scott, K. Cowtan, Features and development of Coot. *Acta crystallographica*, Section D, Biological crystallography 66 (2010) 486–501.
[30] G. Bricogne, E. Blanc, M. Brandl, C. Flensburg, P. Keller, W. Paciorek, P. Roversi, A. Sharff, O.S. Smart, C. Vonrhein, T.O. Womack, BUSTER Version 2.10.3, Global Phasing Ltd, Cambridge, UK, 2017.
[31] P.D. Adams, P.V. Afonine, G. Bunkoczi, V.B. Chen, I.W. Davis, N. Echols, J.J. Headd, L.-W. Hung, G.J. Kapral, R.W. Grosse-Kunstleve, A.J. McCoy, N.W. Moriarty, R. Oeffner, R.J. Read, D.C. Richardson, J.S. Richardson, T.C. Terwilliger, P.H. Zwart, PHENIX: a comprehensive Python-based system for macromolecular structure solution, Acta Crystallogr. Sect. D 66 (2010) 213–221.